SPWLA 60th Annual Logging Symposium, June 15-19, 2019
DOI: 10.30632/T60ALS-2019_KKKKK

ESTIMATION OF DYNAMIC PETROPHYSICAL PROPERTIES FROM MULTIPLE WELL LOGS USING MACHINE LEARNING AND UNSUPERVISED ROCK CLASSIFICATION

Mohamed Bennis and Carlos Torres-Verdín, The University of Texas at Austin

This paper was prepared for presentation at the SPWLA 60th Annual Logging Symposium held in The Woodlands, TX, USA June 17-19, 2019.

ABSTRACT

The process of mud-filtrate invasion gives indirect information about the dynamic petrophysical properties of reservoir rocks, which are essential to predict ultimate hydrocarbon recovery and to optimally design hydrocarbon recovery procedures.

Our focus is on the interpretation of conventional well logs such as density, neutron porosity, and apparent resistivity to estimate dynamic properties of rocks such as permeability and residual hydrocarbon saturation using a machine-learning (ML) algorithm. The inversion problem is mathematically posed as a minimization of a cost function. There exist various approaches to solve this problem such as gradient-based and statistical methods. However, these methods can be computationally expensive, and the process needs to be repeated for each new set of measurements. In this study, we investigate ML methods to automatically detect and extract complex features present in the training dataset.

The dataset is synthetically generated using fast numerical simulations implemented with The University of Texas at Austin Petrophysical and Well-log Simulator (3D UTAPWeLS). We assume a vertical well, horizontal layers, and axial symmetric invasion. Dynamic petrophysical properties of layers are randomly generated using biased distributions. We simulate the process of mud-filtrate invasion and obtain the radial distribution of water saturation and salt concentration. Corresponding well logs such as density, neutron porosity, and apparent resistivity are numerically simulated. This process is repeated until thousands of examples are generated to serve as a database using parallel computations. The performance of the ML model is optimized through the adjustment of hyper-parameters or by adding or removing features.

Several synthetic examples describe the successful application of ML methods on the estimation of dynamic petrophysical properties of hydrocarbon-bearing rocks invaded with water-base mud and water-bearing rocks invaded with oil-base mud. The estimated dynamic petrophysical properties are then used as an input for unsupervised rock classification using hierarchical clustering.

INTRODUCTION

Mud-filtrate invasion takes place under overbalanced drilling conditions. In the case of invasion with oil-base mud (OBM), the invasion process involves immiscible fluid displacement between OBM-filtrate and water, whereby no change in water salinity takes place. In the case of invasion with water-base mud (WBM) filtrate, it is necessary to account for the effect of salt mixing between connate water and mud filtrate.

Depending on the dynamic petrophysical properties of the formation, the displacement of in-situ fluids with mud-filtrate will result in shallow, deep, sharp, or spatially smooth radial fronts of fluid saturation away from the borehole wall (Heidari, 2012). Well-logging tools have different depths of investigation and exhibit varying sensitivity to the radial distribution of petrophysical properties with the formation.

Recent publications emphasize the importance of numerical simulation of mud-filtrate invasion and well logs to estimate static and dynamic petrophysical properties of rock formations (Salazar et al., 2006; Torres-Verdin et al., 2006; Alpak et al., 2008; Malik et al., 2008; Heidari et al., 2011; Salazar et al, 2011; Vandamme et al., 2017). This paper presents a new method to estimate dynamic petrophysical properties based on machine-learning that can potentially accelerate the inversion process.

METHOD

Numerical Simulation of Well Logs of an Invaded Formation

Petrophysical Models. Absolute permeability k is described using Timur-Coates model given by

KKKKK

$$k=\left(a_{TC}\Phi^{b_{TC}}\frac{1-S_{wr}}{S_{wr}}\right)^{c_{TC}} \quad (1)$$

where a_{TC}, b_{TC} and c_{TC} are fitting parameters specific to each rock type, Φ is porosity and S_{wr} is irreducible water saturation (Timur, 1968). Rocks are assumed water-wet, whereas rock-fluid properties such as saturation-dependent capillary pressure and relative permeability are described with parametric Brooks-Corey's equation and Burdine's model (Corey, 1994; Burdine et al., 1953). We assume that these models are valid for both drainage and imbibition conditions. Capillary pressure P_c is given by

$$P_c=P_d S_N^{-\frac{1}{\lambda}}, \quad (2)$$

where P_d is displacement pressure, λ is pore-size distribution exponent, and S_N is normalized water saturation, given by

$$S_N=\frac{S_w-S_{wr}}{1-S_{wr}-S_{hr}}, \quad (3)$$

where S_{hr} is residual hydrocarbon saturation. Water and hydrocarbon saturation-dependent relative permeabilities $k_{rw}$and k_{rh}, respectively, are given by

$$k_{rw}=k_{rw}^0 S_N^2\frac{\int_0^{S_N}\frac{dS_N}{P_c^2}}{\int_0^1\frac{dS_N}{P_c^2}}, \quad (4)$$

and

$$k_{rh}=k_{rh}^0(1-S_N)^2\frac{\int_{S_N}^1\frac{dS_N}{P_c^2}}{\int_0^1\frac{dS_N}{P_c^2}}, \quad (5)$$

where k_{rw}^0 and k_{rh}^0 are relative permeability end points.

Empirical correlations between permeability, porosity and the displacement pressure exist in the literature (Vandamme et al., 2017). In this paper, we introduce a new relationship based on critical path analysis. Katz and Thompson (1987) proposed the relationship

$$k=\frac{1}{c_{KT}}\frac{R_c^2}{F}, \quad (6)$$

where c_{KT} is a constant, F is formation factor, and R_c is the characteristic radius corresponding to threshold pressure P_t. We assume that displacement pressure and threshold pressure are equal. Pore-throat radius and capillary pressure are related through Washburn's equation

$$R=\frac{2\sigma\cos\theta}{P_c}, \quad (7)$$

where R is pore-throat radius, θ is contact angle between fluid interface and pore wall, and σ is interfacial tension. From equation (6) and (7), we derive the following formula

$$P_d=c_p\sqrt{\frac{k}{\Phi^m}}, \quad (8)$$

where c_p is a fitting parameter.

Numerical Simulation of Mud-filtrate Invasion. In this paper, we assume a vertical well, horizontal layers, axial-symmetric invasion, and no hydraulic communication between adjacent beds. Based on the petrophysical relationships described in the previous section, we construct an earth model wherein we populate the necessary inputs for the simulation of mud-filtrate invasion. Drilling parameters such as time of invasion, mudcake properties, and overbalance pressure are also included. Numerical simulation of mud-filtrate invasion is then performed with 3D UTAPWeLS. The outputs of the simulation include the post invasion radial distribution of water saturation and salt concentration. Values of salt concentration are converted to equivalent values of water resistivity R_w using the Dresser Atlas equation (Bigelow, 1992)

$$R_w=(0.0123+\frac{3647.5}{[NaCl]^{0.955}})(\frac{81.77}{T+6.77}), \quad (9)$$

where T is formation temperature in °F and *[NaCl]* is salt concentration in ppm.

Numerical Simulation of Well Logs. The outputs of mud-filtrate invasion simulation are converted to radial distributions of electrical resistivity using Archie's equation; we consider clean rocks without shale. The corresponding resistivity logs are obtained from numerical simulation of array-induction apparent resistivity logs (AIT, mark of Schlumberger). The radial distribution of nuclear properties such as bulk density and migration length are estimated using The University of Texas Nuclear Properties calculator (UTNuPro). Nuclear logs such as density porosity (DPHI) and neutron porosity (NPHI) are then simulated using the wireline Longhorn tool simulator implemented in 3D UTAPWeLS (Mendoza et al., 2010).

Machine Learning Models

The objective of building an ML model is to estimate dynamic petrophysical properties such as permeability and residual hydrocarbon from nuclear and resistivity logs. Different ML models are built depending on the type of mud, the number of input features, and the

KKKKK

number of outputs to be predicted for each case. For instance, in the case of OBM invading a water-saturated formation, nuclear logs are not included as input features because of marginal sensitivity to dynamic properties. Whereas in the case of WBM invading a hydrocarbon-saturated formation, nuclear logs are included as input features because they exhibit sufficient sensitivity to residual hydrocarbon saturation. ML models are scripted in Python using Scikit-Learn libraries (Pedregosa et al., 2011).

Generating Synthetic Data. The first step in developing our machine learning models is to generate the data on which the models will be trained, validated and tested. Dynamic petrophysical properties of layers are randomly generated using biased distributions to ensure that the entire space of neutron porosity log, density porosity log, and the logarithm of apparent resistivity logs is properly covered. The parameters that are sampled from a log-uniform distribution are Φ and S_{wr}. This choice is made based on the multi-linear relationship between $\log(Rt)$, $log(\Phi)$, and $log(S_w)$ in Archie's equation, where Rt is formation electrical resistivity. Remaining parameters such as S_{hr}, λ, k_{rw}^0 and k_{rh}^0 are either fixed to a specific value or sampled from a uniform distribution. The post-invasion radial distributions of petrophysical properties are used to compute the apparent resistivity and nuclear logs for each sample. This process is repeated until thousands of samples are generated using parallel computations. **Figure 1** summarizes the different steps used for generating the synthetic data for each set of petrophysical parameters.

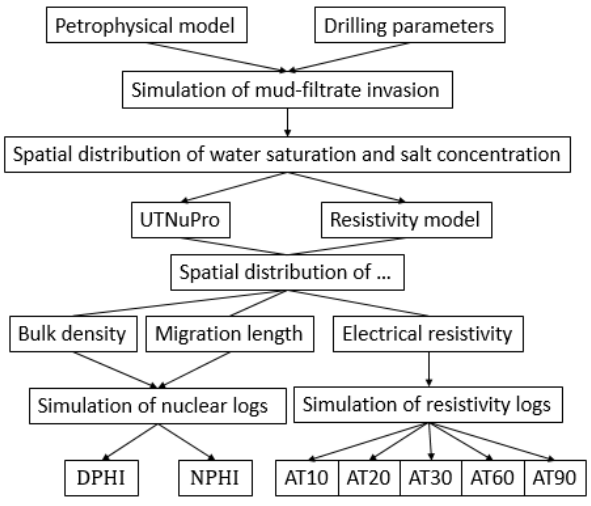

Figure 1: - Adopted workflow to generate synthetic well log data.

Decision Trees and Random Forests. Multiple ML methods exist for regression problems. In this paper, we apply decision trees to construct an estimator that predicts the value of one or multiple target variables by learning decision rules learned from data features. Decisions trees can be unstable because small variations in the data might result in a completely different tree being generated. This problem is mitigated by using decision trees within an ensemble called random forests. In this paper, we use one hundred trees per model. In addition, decision trees are prone to over-fitting, especially when a tree is particularly deep. We mitigate this problem by tuning the hyper-parameters of the estimator by setting a maximum depth. Other methods were tested such as neural networks and in our cases, decision trees yield better predictions. Unlike neural networks, decision trees do not require data normalization and have less hyper-parameters to optimize.

Evaluating ML Model Performance. We divide the dataset into three disjoint subsets denoted as training, validation, and test. Given the training and test sets, we compare the performance of different decision trees. Then, we verify the accuracy of our approximation on the validation dataset. If the accuracy is insufficient, we build a new enhanced ML model to reduce the error. The performance of the ML model is optimized through the adjustment of the hyper-parameters or by adding or removing features. New features are incorporated such as the ratio of deep to shallow resistivity logs and the average of neutron porosity and density porosity logs.

The performance of ML models is assessed via two measures. The coefficient of determination R^2 is a measurement of correlation between predictions and true values. If Y_i is the predicted value of the i-th sample and y_i is the corresponding true value, then the score R^2 estimated over $n_{samples}$ is computed as

$$R^2(y,Y) = 1 - \frac{\sum_{i=1}^{n_{samples}} (y_i - Y_i)^2}{\sum_{i=1}^{n_{samples}} (y_i - \bar{y})^2}, \quad (10)$$

where

$$\bar{y} = \frac{1}{n_{samples}} \sum_{i=1}^{n_{samples}} y_i. \quad (11)$$

The mean squared error (MSE) corresponds to the standard deviation of the residuals. In other words, it indicates how concentrated the data are around the line of best fit. The score MSE estimated over $n_{samples}$ is computed as

$$MSE(y,Y) = \frac{1}{n_{samples}} \sum_{i=1}^{n_{samples}} (y_i - Y_i)^2. \quad (12)$$

KKKKK

Because the training dataset is synthetically constructed, we can hypothetically generate an infinite number of training samples. However, generating synthetic data has a cost. On a desktop computer with i7-370 CPU @3.40 GHz and 32.0 GB of memory (RAM), we are currently able to generate 8 samples per minute. The visualization of a learning curve is one way we use to determine how much we benefit from adding more training data. A learning curve shows the training and validation score of an ML model that learns from a training dataset incrementally.

SYNTHETIC CASE NO. 1: ESTIMATION OF PERMEABILITY IN A WATER-SATURATED FORMATION INVADED BY OBM

Synthetic case No.1 is constructed based on field data from a water-saturated sandstone reservoir invaded with OBM. **Table 1** lists formation properties and drilling parameters. This synthetic example is intended to examine the sensitivity of resistivity logs to porosity and permeability and to illustrate how the ML model is constructed and tested. Finally, we construct a multilayer synthetic example to assess the uncertainty of permeability predictions.

Table 1: Summary of mudcake and formation properties assumed in the simulation of the process of mud-filtrate invasion.

Variable	Units	Value
Wellbore radius	m	0.1
Invasion time	days	3
Overbalance pressure	psi	300
Reservoir temperature	F	165
Reservoir external radius	m	20
Mudcake reference permeability	mD	0.03
Mudcake reference porosity	frac	0.35
Mud solid fraction	frac	0.06
Mudcake maximum thickness	inch	0.4
Mudcake compressibility exponent	frac	0.4
Mudcake exponent multiplier	frac	0.1

Sensitivity of the Radial Profile of Water Saturation and the Electrical Resistivity Logs to Permeability. We set porosity to 20%, vary permeability in the range from 0.2 to 2000 mD, and numerically simulate mud-filtrate invasion and the corresponding apparent resistivity logs. **Figure 2** shows the radial distribution of water saturation around the borehole and **Figure 3** shows the sensitivity of the separation between resistivity logs array-induction resistivity logs to permeability. For permeability values lower than a threshold value of 30 mD, the separation between resistivity logs increases with an increase of permeability. For permeability values larger than 30 mD, the separation between resistivity logs decreases with an increase of permeability. The threshold value varies as a function of formation porosity. This phenomenon is explained by the fact that the process of mud filtrate invasion is jointly controlled by formation rock properties and mud-cake properties (Wu et al., 2005).

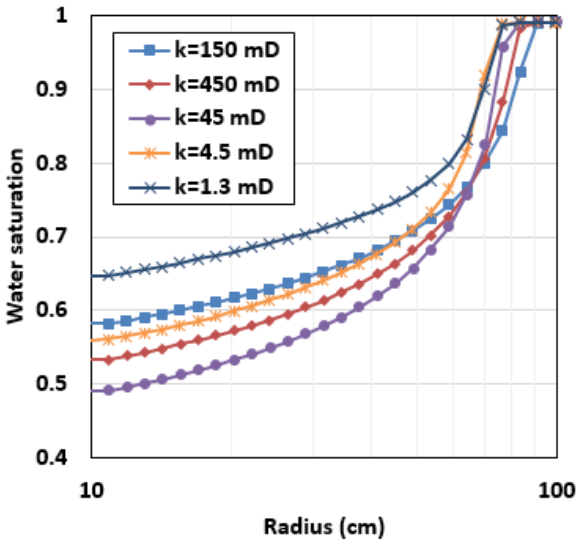

Figure 2: - Radial profile of water saturation for varying irreducible water saturation values.

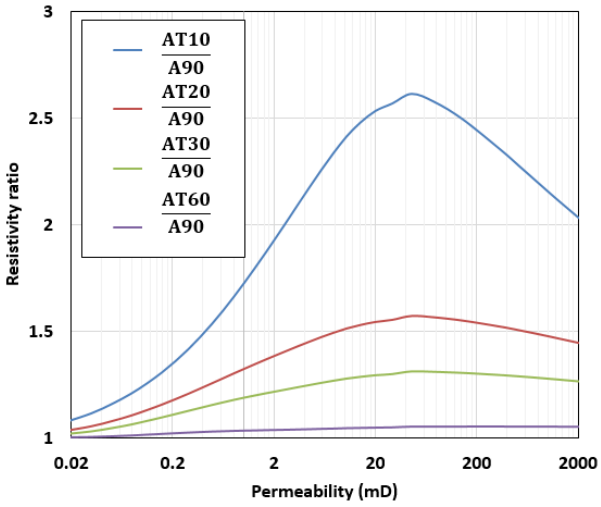

Figure 3: Resistivity ratio between shallow and deep resistivity logs.

KKKKK

Sensitivity of Apparent Resistivity Measurements to Porosity. We vary porosity from 5% to 35%. and numerically simulate mud-filtrate invasion and the corresponding apparent resistivity logs. **Figure 4** shows that low porosity rocks exhibit the largest separation between resistivity logs, and hence they exhibit the largest sensitivity to permeability.

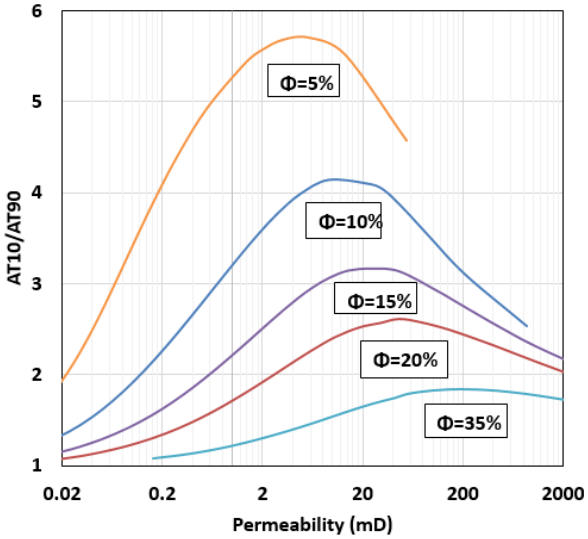

Figure 4: - Sensitivity of resistivity ratio AT10/AT90 for varying porosity values.

Generating Synthetic Data. For each data sample, porosity is randomly sampled from a log-uniform distribution within the interval [10%, 20%] and irreducible water saturation randomly sampled from a log-uniform distribution within the interval [10%, 50%]. Absolute permeability, capillary pressure, and relative permeability curves are calculated using eqs. (1-5) and (8). These petrophysical parameters are populated in an earth model and the process of mud-filtrate invasion is simulated. Finally, we simulate the induction resistivity tool to obtain apparent resistivity measurements. More than 6800 samples are generated. **Figure 4** shows the distribution of the synthetically generated samples aimed to properly cover to the entire space of interest.

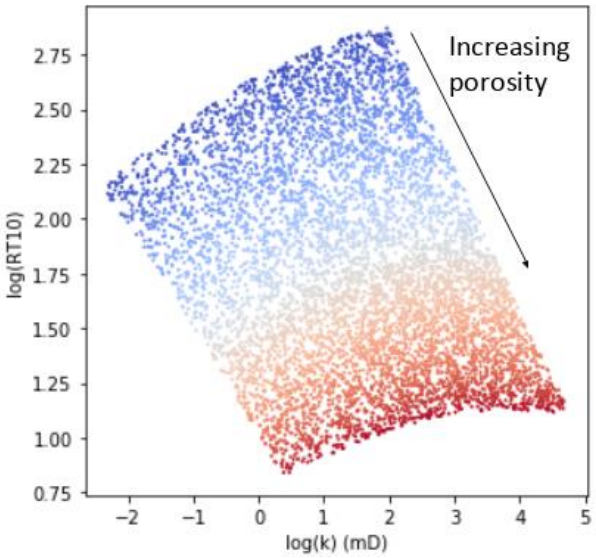

Figure 5: Cross-plot of shallow induction resistivity and permeability for data samples.

Constructing an ML Model. The inputs of the ML model are porosity and the logarithm of apparent resistivity logs AT10, AT20, AT30, AT60, and AT90. The output of the ML model is the logarithm of permeability. **Figures 6** and **7** show cross-plots of ML model predictions and trues values of permeability on training and test data.

KKKKK

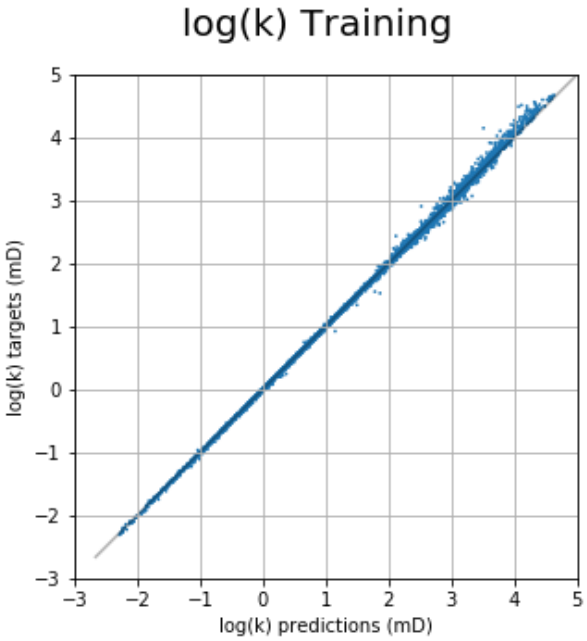

Figure 6: Cross-plot of ML model predictions against target values of the logarithm of permeability on the training set.

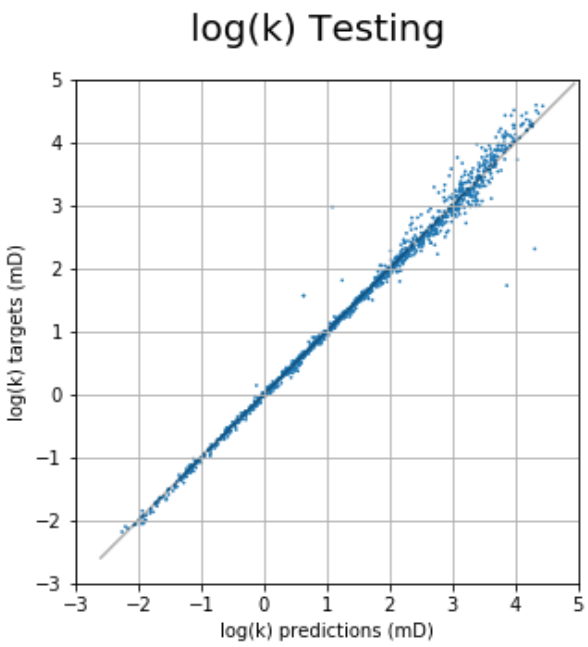

Figure 7: Cross-plot of ML model predictions against target values of the logarithm of permeability on the testing set.

The R^2 and *MSE* scores of the ML model are listed in **Table 2**. The learning curve in **Figure 8** suggests that the R^2 score is above 0.98 when the training size is above 2000 samples.

Table 2: Summary of scores of the ML model.

	Training Log(k)	Testing Log(k)
R^2	0.999	0.990
MSE	0.002	0.023

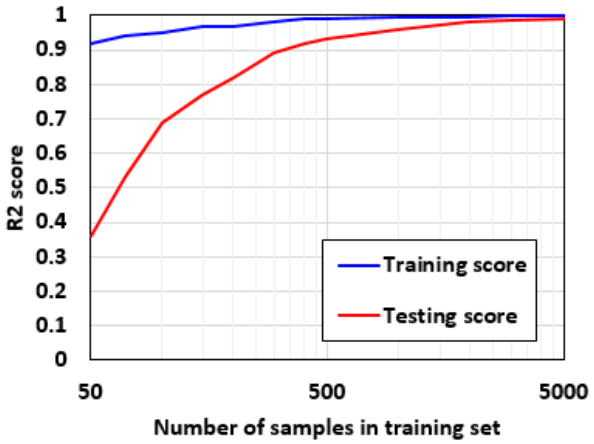

Figure 8: Learning curve showing that the training and testing scores converge to 1 as more training examples are added.

Multi-layer Synthetic Example. We create a 6-layer water-saturated formation with varying porosity and permeability (**Figure 9**). Using the pre-trained ML model, we estimate permeability at the center of the layers where shoulder-bed effects are negligible. The predicted permeability from the ML model shows a good agreement with true layer permeability (**Figure 10**). Layers with large porosity and permeability exhibit larger uncertainty compared to layer with low porosity and permeability. In the case of a multi-layer field example, the input of the ML model would be porosity estimated from conventional multi-mineral analysis and resistivity logs from field measurements.

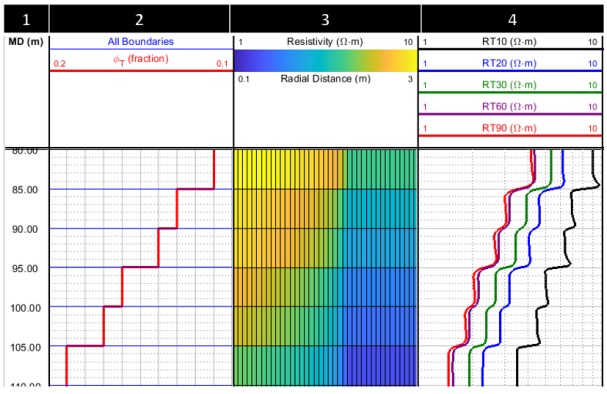

Figure 9: Track 1: Depth. Track 2: Porosity. Track 3: Radial distribution of formation resistivity. Track 4: Induction electrical resistivity logs.

KKKKK

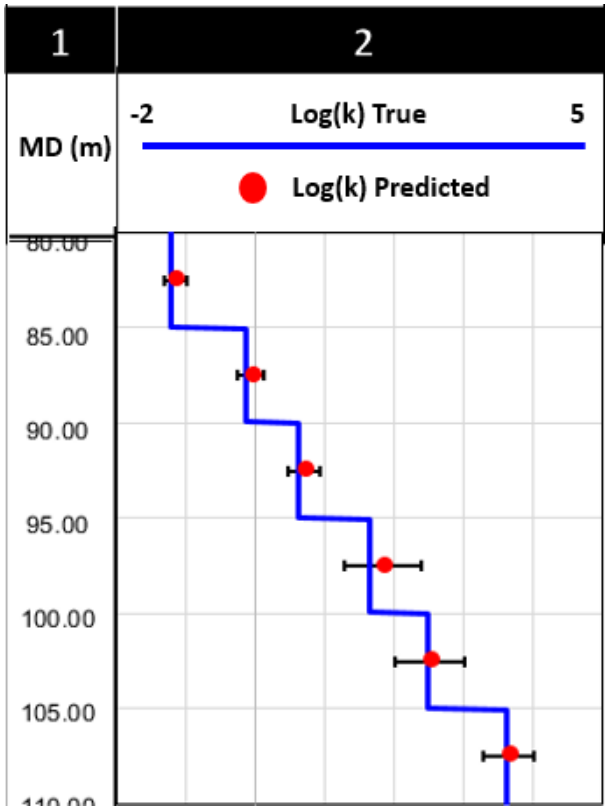

Figure 10: Track 1: Depth. Track 2: True value of the logarithm of permeability and predicted value of the logarithm of permeability.

SYNTHETIC CASE NO. 2: ESTIMATION OF PERMEABILITY AND RESIDUAL HYDROCARBON SATURATION IN A GAS-SATURATED FORMATION INVADED BY WBM

Synthetic Case No.2 is constructed with the same petrophysical parameters as synthetic case No.1. The initial water saturation is assumed to be equal to irreducible water saturation. The hydrocarbon type assumed is methane. This synthetic example is intended to examine the sensitivity of resistivity and nuclear logs to permeability and residual hydrocarbon saturation. The ML model is tested on a multilayer synthetic example to assess the uncertainty of permeability and residual hydrocarbon predictions.

Generating Synthetic Data. For each data sample, irreducible water saturation randomly sampled from a log-uniform distribution within the interval [10% , 50%] and residual hydrocarbon saturation is sampled from a uniform distribution within the interval [10% , $1 - S_{wr}$]. Porosity is set equal to 15%. In this case, mud-filtrate salinity is assumed to be similar to connate water salinity. Absolute permeability, capillary pressure, and relative permeability curves are calculated using eqs. (1-5) and (8). These petrophysical parameters are then populated to create an earth model and the process of mud-filtrate invasion is simulated. Finally, we simulate the induction resistivity tool and the wireline Longhorn nuclear tools to obtain apparent resistivity and nuclear measurements. More than 700 samples are generated.

Constructing an ML Model. The inputs of the ML model are porosity, neutron porosity log (NPHI), density porosity log (DPHI), and the logarithm of apparent resistivity logs AT10, AT20, AT30, AT60, and AT90. The outputs of the ML model are the logarithm of permeability and residual hydrocarbon saturation. **Figures 11, 12, 13** and **14** show cross-plots of ML model predictions and trues values of permeability and residual hydrocarbon saturation on training and test data. The $R^2$and *MSE* scores of the ML model are listed in **Table 2**.

KKKKK

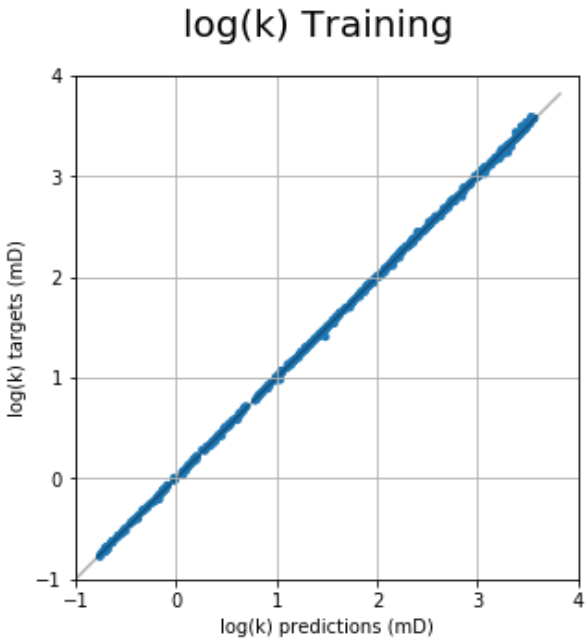

Figure 11: Cross-plot of ML model predictions against target values of the logarithm of permeability on the training set.

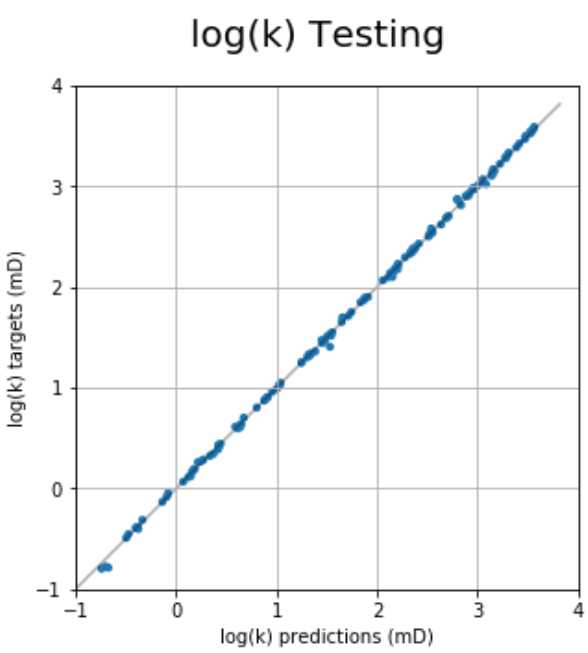

Figure 12: Cross-plot of ML model predictions against target values of the logarithm of permeability on the testing set.

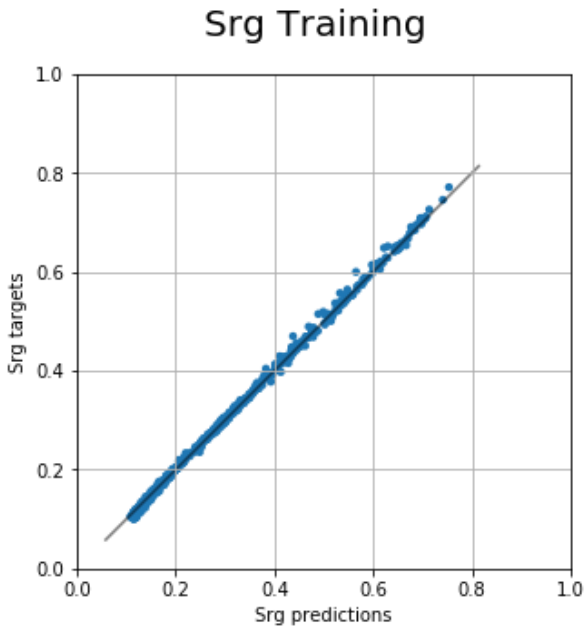

Figure 13: Cross-plot of ML model predictions against target values of residual hydrocarbon saturation on the training set.

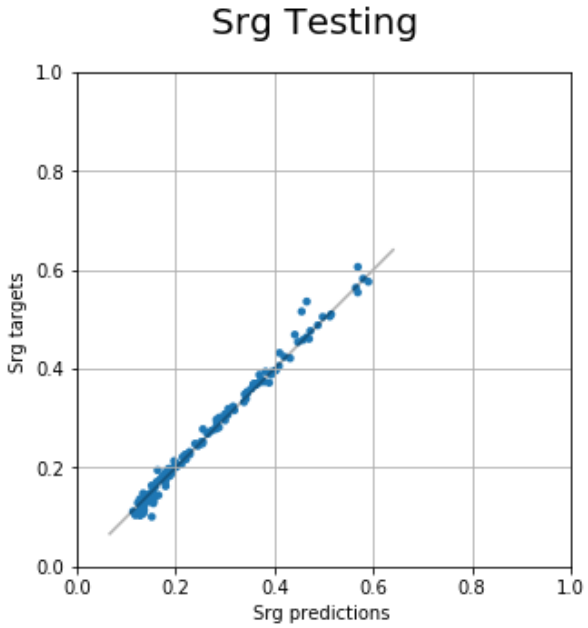

Figure 14: Cross-plot of ML model predictions against target values of residual hydrocarbon saturation on the testing set.

Table 3: Summary of scores of the ML model

	Training Log(k)	Training S_{rg}	Testing Log(k)	Testing S_{rg}
R^2	0.999	0.998	0.999	0.988
MSE	0.0002	0.0001	0.0006	0.0002

Multi-layer Synthetic Example. We create a 6-layer gas-saturated formation with varying permeability and residual hydrocarbon saturation (**Figure 15**). Results are shown in **Figure 16**.

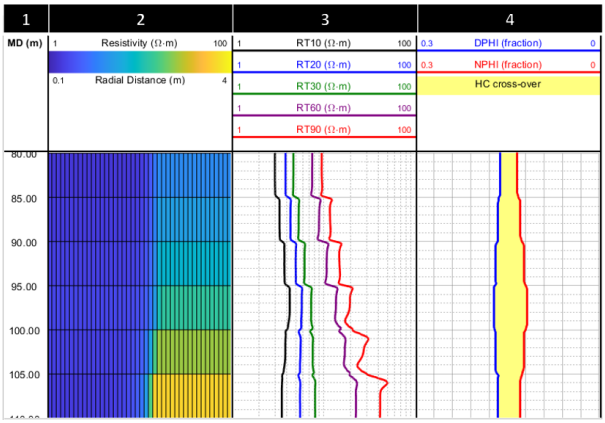

Figure 15: Track 1: Depth. Track 2: Radial distribution of formation resistivity. Track 3: Induction electrical resistivity logs. Track 4: Neutron and density porosity logs.

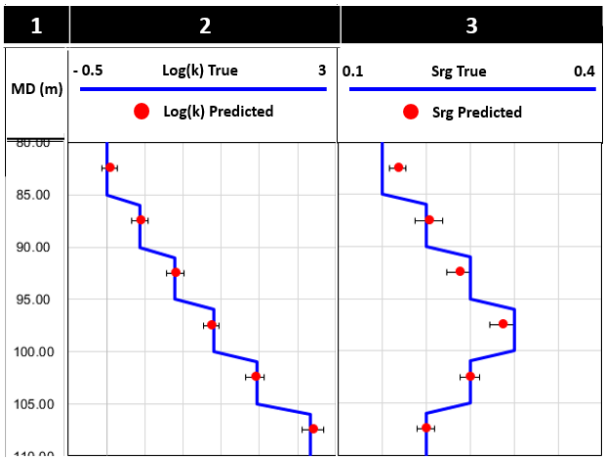

Figure 16: Track 1: Depth. Track 2: True value of the logarithm of permeability and predicted value of the logarithm of permeability. Track 3: True value of residual hydrocarbon saturation and predicted value of residual hydrocarbon saturation.

ASSESSMENT OF ROCK QUALITY

The output of ML models can be used as input of an unsupervised rock classification algorithm such as hierarchical clustering (Xu et al., 2012). In the case of OBM invading water-saturated formation, one can classify rocks based on the estimated Leverett's Rock Quality Index (RQI) given by

$$RQI = \sqrt{k/\Phi}\,, \tag{13}$$

In the case of WBM invading hydrocarbon-saturated formation, one can classify rocks based on the estimated Rock Quality Index (RQI) and the estimated volume of moveable hydrocarbons defined given by

$$V_{moveable} = \Phi * (1 - S_{wr} - S_{rg})\,. \tag{14}$$

CONCLUSIONS

Using ML models, we built an approximation to the inversion function offline. This function can be rapidly evaluated for real-time inversion of well logs across many wells in the same hydrocarbon field. The application of the ML algorithm requires some prior knowledge of drilling mud properties, and for each mud KKKKK configuration we are required to train a new ML model.

Verification exercises performed with synthetic data sets indicate that the ML procedure can be used for fast and reliable estimation of permeability and residual hydrocarbon saturation, for instance, by making use of the effects of mud-filtrate invasion on the available resistivity and nuclear well logs.

ACKNOWLEDMENTS

The work reported in this paper was funded by the University of Texas at Austin's Research Consortium on Formation Evaluation, jointly sponsored by Anadarko, Aramco, Baker Hughes, BHP Billiton, BP, Chevron, ConocoPhillips, COSL, DEA, ENI, Equinor ASA, ExxonMobil, Halliburton, INPEX, Lundin-Norway, Nexen-CNOOC, Oil Search Alaska, Petrobras, Repsol, Schlumberger, Shell, Southwestern Energy, TOTAL, Woodside, and Wintershall.

LIST OF ACRONYMS

AIT	Array Induction Tool
OBM	Oil-Base Mud
WBM	Water-Base Mud
ML	Machine Learning

DPHI	Density porosity log
NPHI	Neutron porosity log
RQI	Leverett's reservoir quality index, $\sqrt{k/\Phi}$

LIST OF SYMBOLS

a_{TC}	Coefficient in Timur-Coates equation
b_{TC}	Coefficient in Timur-Coates equation
c_{TC}	Coefficient in Timur-Coates equation
k	Absolute permeability, (mD)
Φ	Porosity, (frac)
S_{wr}	Irreducible water saturation, (frac)
P_c	Reservoir capillary pressure, (psi)
P_d	Displacement pressure, (psi)
P_t	Threshold pressure, (psi)
S_N	Normalized water saturation, (frac)
S_w	Water saturation, (frac)
λ	Pore-size distribution exponent
k_{rw}	Wetting-phase relative permeability
k_{rw}^0	Wetting-phase relative permeability end-point
k_{rh}	Non-wetting phase relative permeability
k_{rh}^0	Non-wetting phase relative permeability end-point
R	Pore-throat radius, (μm)
R_c	Characteristic radius pore-throat radius (μm)
c_{KT}	Coefficient of Katz-Thompson equation
m	Cementation exponent in Archie's equation
c_p	Coefficient of displacement pressure equation
R_t	formation resistivity, (Ω.m)
R_w	Connate water resistivity, (Ω.m)
$[N_aCl]$	Salt concentration, (ppm)
σ	Interfacial tension, (dyne)
$cos\theta$	Cosine of contact angle

REFERENCES

Alpak, F. O., Torres-Verdín, C., Habashy, T. M., and Sepehrnoori, K., 2008, Estimation of in situ petrophysical properties from wireline formation tester and induction logging measurements: A joint inversion approach, Journal of Petroleum Science and Engineering, Vol. 63, no. 1–4, p. 1–17, doi: 10.1016/j.petrol.2008.05.007.

Burdine, N. T., 1953, Relative permeability calculations from pore size distribution data, Trans. AIME, Vol. 198, no. 71.

Corey, A. T., 1994, Mechanics of immiscible fluids in porous media, Water Resources Publications.

Heidari, Z., Torres-Verdín, C., Mendoza, A., and Wang, G. L., 2011, Assessment of residual hydrocarbon saturation with the combined quantitative interpretation of resistivity and nuclear logs, Petrophysics, Vol. 52, p. 217–237.

Heidari, Z., and Torres-Verdín, C., 2012, Estimation of dynamic petrophysical properties of water-bearing sands invaded with oil-base mud from the interpretation of multiple borehole geophysical measurements, Geophysics, Vol. 77, no. 6, D209-D227

Katz, A. J. and Thompson, A. H., 1987, Prediction of electrical conductivity from mercury injection measurements, Journal of geological research, Vol. 92, no. B1, p. 599-607.

Malik, M., Salazar, J.M., Torres-Verdín, C., Wang, G. L., Lee, H. J. and Sepehrnoori, K., 2008, Effects of petrophysical properties on array-induction measurements acquired in the presence of oil-base mud-filtrate invasion, Petrophysics, Vol. 49, p. 74–92.

Mendoza, A., Torres-Verdín, C., and Preeg, W.E., 2010, Linear iterative refinement method for the rapid simulation of borehole nuclear measurements, Part I: Vertical wells: Geophysics, Vol. 75, no. 1, E9–E29, doi: 10 .1190/1.3267877.

Salazar, J. M., Torres-Verdín, C., Alpak, F.O., Habashy, T. M., and Klein, J. D., 2006, Estimation of permeability from array induction measurements: Applications to the petrophysical assessment of tight-gas sands, Petrophysics, Vol. 47, p. 527–544.

Salazar, J. M., Torres-Verdín, C., and Wang, G. L., 2011, Effects of surfactant emulsified oil-based mud on borehole resistivity measurements, SPE Journal, Vol. 16, p. 608–624, doi: 10.2118/109946-PA.

Scikit-learn: Machine Learning in Python, Pedregosa et al., JMLR 12, pp. 2825-2830, 2011.

Timur, A., 1968, An investigation of permeability, porosity, and residual water saturation relationship for sandstone reservoirs, The Log Analyst, Vol. 9, no. 4, p. 8–17.

Torres-Verdín, C., Alpak, F.O., and Habashy, T. M., 2006, Petrophysical inversion of borehole array-induction logs. Part II-Field data examples, Geophysics, Vol. 71, no. 5, G261-G268.

KKKKK

Wu, J., Torres-Verdín, C., Sepehrnoori, K., and Proett, M. A., 2005, The influence of water-base mud properties and petrophysical parameters on mudcake growth, filtrate invasion, and formation pressure, Petrophysics, Vol. 46, no. 1, p. 14-32.

Xu, C., and Torres-Verdín, C., 2012, Saturation-height and invasion consistent hydraulic rock typing using multi-well conventional logs, SPWLA 53rd Annual Logging Symposium.

ABOUT THE AUTHORS

Mohamed Bennis is a Ph.D. candidate in the Hildebrand Department of Petroleum and Geosystems and a Graduate Research Assistant in the Formation Evaluation Consortium Research Program at The University of Texas at Austin. He received his M.Sc. in in engineering from École Centrale de Lille. He is currently an officer of The SPWLA Student Chapter at The University of Texas at Austin.

Carlos Torres-Verdín received a Ph.D. in Engineering Geoscience from the University of California at Berkeley in 1991. During 1991-1997, he held the position of Research Scientist with Schlumberger-Doll Research. From 1997-1999, he was Reservoir Specialist and Technology Champion with YPF (Buenos Aires, Argentina). Since 1999, Dr. Torres-Verdín has been affiliated with the Department of Petroleum and Geosystems Engineering of the University of Texas at Austin, where he is currently Full Professor, and holds the Brian James Jennings Memorial Endowed Chair in Petroleum and Geosystems Engineering. Dr. Torres-Verdín is the founder and director of the Research Consortium on Formation Evaluation at the University of Texas at Austin. He is the recipient of the Cockrell School of Engineering's 2016-2017 Lockheed Martin Aeronautics Company Award for Excellence in Engineering Teaching, the 2014 Gold Medal for Technical Achievement from the SPWLA, the 2008 Formation Evaluation Award from the SPE, and the 2006 Distinguished Technical Achievement Award from the SPWLA. He is a Distinguished Member of the Society of Petroleum Engineers (SPE), Honorary Member of the Society of Exploration Geophysicists (SEG), and receiver of the Conrad Schlumberger Award from the European Association of Geoscientists and Engineers (EAGE).

KKKKK